SLC13A5 plays an essential role in the energy shift to oxidative phosphorylation in cisplatin-resistant mesothelioma stem cells

Marie Kato-Shinomiya[1], Hirokazu Sugino[1,2], Lei Wang[1,3], Yusuke Saito[1,4], Jintao He[1], Zen-ichi Tanei[1,5], Yoshitaka Oda[1], Satoshi Tanikawa[1,6], Mishie Tanino[7], Jian Ping Gong[3,8], Masumi Tsuda[1,3,*], Shinya Tanaka[1,3,5]

[1] Department of Cancer Pathology, Faculty of Medicine, Hokkaido University, Sapporo, Japan
[2] Department of Diagnostic Pathology, National Cancer Center Hospital, Tokyo, Japan
[3] Institute for Chemical Reaction Design and Discovery (WPI-ICReDD), Hokkaido University, Sapporo, Japan
[4] Division of Clinical Cancer Genomics, Hokkaido University Hospital, Sapporo, Japan
[5] Department of Surgical Pathology, Hokkaido University Hospital, Sapporo, Japan
[6] Department of Laboratory Medicine and Pathobiology, Tanz Centre for Research in Neurodegenerative Disease, University of Toronto, Toronto, Canada
[7] Department of Diagnostic Pathology, Asahikawa Medical University Hospital, Asahikawa, Japan
[8] Faculty of Advanced Life Science, Hokkaido University, Sapporo, Japan

Cocorresponding authors:
Masumi Tsuda, Ph.D.
Department of Cancer Pathology, Faculty of Medicine, Hokkaido University, North 15 West 7, Kita-ku, Sapporo, Hokkaido, 068-8638, Japan
Tel: +81-11-706-7806
Fax: +81-11-706-5902
E-mail: tsudam@med.hokudai.ac.jp

Keywords

SLC13A5, mesothelioma, cancer stem cell, hydrogel, reprogramming

Abstract

Mesothelioma is a highly aggressive tumor affecting an increasing number of patients worldwide. Owing to the poor clinical outcomes associated with current therapies, the development of novel therapies that target cancer stem cells (CSCs) is desirable. Here, we examined the applicability of our previously established hydrogel-based rapid CSC generation method to human mesothelioma cell lines and further analyzed the characteristics of the induced mesothelioma stem-like cells (MesoSCs). Human mesothelioma cell lines cultured on hydrogels presented increased expression of panstem cell markers and acquired spheroid formation and early tumorigenicity, suggesting that MesoSCs are highly malignant. Microarray analysis demonstrated that the expression of *SLC13A5*, a citrate transporter involved in TCA cycle, was significantly induced in the resulting MesoSCs. The overexpression of SLC13A5 resulted in a metabolic shift toward oxidative phosphorylation, increased phosphorylation of ERK and YAP, and increased SOX2 expression, leading to increased cisplatin resistance. scRNA-seq database analysis revealed that clinical mesothelioma samples contained a small number of SLC13A5-expressing cells. Our findings suggest that the hydrogel-based CSC generation method is also effective for human mesothelioma cells and that SLC13A5 may contribute to MesoSC survival. The new properties of MesoSCs revealed in this study may provide clues for establishing future treatments.

Introduction

Mesothelioma is a highly aggressive tumor associated with risk factors such as asbestos and BAP1 gene mutations and it develops after a latency period of several decades after initial exposure [1–3]. Although the number of patients worldwide has increased every year since 1990, its prevalence has already peaked in Europe and in the United States, and it is predicted that all mesothelioma cases will be spontaneous rather than asbestos-induced by 2040 [4, 5]. Surgical resection is the first choice of treatment, but due to the complex anatomy, up to 75% of patients experience local recurrence [6]. Recurrent or unresectable cases can be treated with chemotherapy [7, 8], radiotherapy [9], and immunotherapy [10–12], but all of these treatments are associated with poor clinical outcomes.

Cancers are composed of heterogeneous cell populations and are often difficult to cure because of the presence of cancer stem cells (CSCs), which are involved in metastasis and drug resistance [13–15]. To eradicate CSCs, it is essential to isolate CSCs from cancer tissues, analyze their characteristics, and develop CSC-targeted therapies. In mesothelioma, mesothelioma stem cells (MesoSCs) are selected by sorting cells with high expression of SOX2 and Oct4 via lentivirus [16] or by sorting side population cells that show superior responses to dye exclusion or the Aldefluor assay [17, 18]. These methods revealed that in MesoSCs, SOX2, Nanog, and Oct4 are involved in multipotency [19]; CD9, CD24, and CD26 are involved in tumorigenesis and invasion [18, 20]; and CD44 and ALDH are involved in drug resistance [21, 22]. However, these conventional methods inevitably lead to nonphysiological conditions due to the addition of viruses or reagents to cells, and the high reagent costs, complicated procedures, and low isolation efficiency are barriers to the development of MesoSC-targeted therapies.

To address this issue, we recently established a novel method to rapidly reprogram cancer cells into CSCs via a hydrogel, termed the hydrogel-activated reprogramming (HARP) phenomenon [23]. Hydrogels have the advantage that their high water content allows cancer cells to be cultured in a microenvironment similar to that *in vivo*, without the need for expensive reagents and equipment. Indeed, we have succeeded in rapidly reprogramming brain tumor cell lines into glioma stem cells via a double network (DN) hydrogel composed of poly(2-acrylamido-2-methyl-1-propanesulfonic acid) (PAMPS) and poly(*N*,*N'*-dimethylacrylamide) (PDMAAm) [23–25]. Recently, we reported that poly(N-(carboxylmethyl)-N,N'-dimethyl-2-(methacryloyloxy)ethanaminium, inner salt) (PCDME) gel [26, 27] and poly(sodium *p*-styrene sulfonate) (PNaSS) gel [28] are also able to upregulate pan-stem cell markers in various malignant tumor cell lines (unpublished data).

Mesothelial cells are generated by epithelialization of the lateral mesoderm and provide a special intermediate context between mesenchymal and epithelial cells [29, 30]. Mesotheliomas develop in a membranous fashion and rarely form masses, suggesting that they may be a distinct cell type from other malignancies embryologically, anatomically, and histologically. Activation of the Hippo pathway and osteopontin production in mesothelioma cells have been reported to contribute to stemness and drug resistance [31–33], and it is expected that these cells will be sensitive to extracellular mechanical stimuli, suggesting that hydrogels may be able to induce MesoSCs similar to other malignancies. In this study, we investigated the applicability of human mesothelioma cell lines for hydrogel-based CSC induction. Furthermore, we noted the increased expression of *SLAC13A5*, a gene encoding a citrate transporter, in the obtained MesoSCs and analyzed its contribution to MesoSC survival. We hope that

the properties of MesoSCs that we uncovered could provide a foothold for novel therapeutic approaches.

2. Materials and Methods

2.1 Cell lines

Human mesothelioma cell line ACC-MESO-4 [34] and human embryonic kidney cell line HEK293T were provided by the RIKEN BioResearch Center (Tukuba, Japan). Other four human mesothelioma cell lines MSTO-211H, NCI-H2052, NCI-H2452 and NCI-H28 were purchased from the American Type Culture Collection (ATCC, Manassas, VA, USA).

2.2 Cell culture

All mesothelioma cell lines were maintained in Roswell Park Memorial Institute (RPMI) 1640 medium (Nissui Pharmaceutical, Tokyo, Japan) with 10% fetal bovine serum (FBS, Sigma-Aldrich, St. Louis, MO, USA), penicillin-streptomycin (100 U/mL penicillin and 0.1 mg/mL streptomycin, Sigma-Aldrich, St. Louis, MO, USA), and L-glutamine (2 mM, Sigma-Aldrich, St. Louis, MO, USA). HEK293T cells were maintained in Dulbecco's Modified Eagle Medium (DMEM) with 10% FBS, penicillin-streptomycin, and L-glutamine. All cell lines were cultured on hydrogels or polystyrene (PS) dish at 37°C in a humid incubator with 5% CO_2.

2.3 Establishment of ACC-MESO-4 and MSTO-211H cells stably expressing tdTOMATO-Luc2

pCSII-CMV-tdTOMATO-Luc2 was transfected into ACC-MESO-4 and MSTO-211H

cells using FuGENE® HD transfection reagent (Promega, Madison, WI, USA), and the transfected cells were selected in the presence of 200 ng/mL Zeocin (Thermo Fisher Scientific, Waltham, MA, USA). Stable expression of tdTOMATO fluorescent protein was observed under a fluorescence microscope (IX73, Olympus, Co., Tokyo, Japan). In the established cells, increased expression of pan-stem cell markers on DN, PCDME, and PNaSS gels was confirmed to be equivalent to those of the parental cells, demonstrating no adverse effects of fluorescent protein.

2.4 Establishment of cell lines transiently overexpressing SLC13A5

SLC13A5 expression vector (pRP[Exp]-EGFP/Puro-EF1A>3xFLAG/hSLC13A5 [NM_177550.5]) and its empty control vector (EGFP control vector pRP[Exp]-EGFP/Puro-CAG> ORF_stuffer) were purchased from Vector Builder Inc. (Chicago, IL, USA). ACC-MESO-4 cells were seeded at 1.0×10^5 cells/mL, MSTO-211H cells and HEK293T cells at 2.5×10^5 cells/mL on a PS dish, and 2000 μg of SLC13A5 expression vector or empty control vector were transfected using FuGENE® HD. After 48 hours of transfection, the transfection efficiency was evaluated by the expression of green fluorescent protein under an IX73 inverted microscope.

2.5 Synthesis of hydrogels

Hydrogel regents

As monomers for hydrogels, we purchased 2-acrylamido-2-methyl-1-propanesulfonic acid (AMPS, Toagosei Co., Ltd., Tokyo, Japan), N,N'-dimethylacrylamide (DMAAm, FUJIFILM Wako Pure Chemical Co., Osaka, Japan), N-(Carboxylmethyl)-N,N'-dimethyl-2-(methacryloyloxy)ethanaminium, inner salt (CDME, Osaka Organic

Chemical Co., Ltd., Osaka, Japan) and p-styrenesulfonic acid sodium salt (FUJIFILM Wako Pure Chemical Co.). N, N'-methylenebisacrylamide (MBAA, FUJIFILM Wako Pure Chemical Co.) was used as a cross-linking agent and 2-oxoglutaric acid (FUJIFILM Wako Pure Chemical Co.) was used for polymerization initiator. All agents except DMAAm were used without further purification. DMAAm was used after vacuum distillation.

DN gel synthesis

The PAMPS/PDMAAm DN gel was synthesized with APMS, DMAAm, MBAA, and 2-oxoglutaric acid following a previously reported 2-step sequential polymerization method [24]. The structural formulas for PAMPS and PDMAAm are shown in **Figure 1A**. First, to make a first network of PAMPS hydrogel, we prepared a precursor solution, which contains 1 mol/L AMPS, 4 mol% MBAA and 0.1 mol% 2-oxoglutaric acid. This precursor solution was injected into a cell consisting of a pair of glass plates separated by silicone rubber. When the cell is irradiated with ultraviolet (UV) lamp (365 nm wavelength) in argon gas for about 8 hours, PAMPS gel is synthesized by radical polymerization. Next, the PAMPS hydrogel was immersed in a 2 mol/L DMAAm solution containing 0.1 mol% MBAA and 0.1 mol% 2-oxoglutaric acid for 1 day until achieving the equilibrium. The hydrogel was then put between two glass plates and irradiated with a UV lamp (365 nm wavelength) in argon gas for about 8 hours. This resulted in polymerization of the second network (PDMAAm) in the presence of the first network gel (PAMPS) to obtain DN gel [24].

PCDME gel synthesis

PCDME gel was obtained by radical polymerization using precursor solution containing 1 mol/L N-(Carboxylmethyl)-N,N'-dimethyl-2-(methacryloyloxy)ethanaminium, inner salt, 4 mol% MBAA, and 0.1 mol% 2-oxoglutaric acid. The solution was injected into a cell consisting of a pair of glass plates separated by silicone rubber. The cell was irradiated with a UV lamp (365 nm wavelength) in argon gas for about 8 hours [26].

PNaSS gel synthesis

PNaSS gel was obtained by radical polymerization using precursor solution containing 1 mol/L p-styrenesulfonic acid sodium salt, 4 mol% MBAA, and 0.1 mol% 2-oxoglutaric acid. The solution was injected into a cell consisting of a pair of glass plates separated by silicone rubber. The cell was irradiated with a UV lamp (365 nm wavelength) in argon gas for about 9 hours [28].

After polymerization, DN gel, PCDME gel and PNaSS gel were immersed in 0.9 wt% NaCl solution to remove unreacted material, and then further immersed in 4-(2-HydroxyEthyl)-1-Piperazine Ethane Sulfonic acid (HEPES, Sigma-Aldrich, St. Louis, MO, USA) buffer［1.55×10^{-2} mol/L $NaHCO_3$, 0.14 mol/L NaCl, 5×10^{-3} mol/L HEPES, pH 7.4]. The HEPES buffer was replaced daily for 1 week, and these hydrogels reaching equilibrium were used for cell culture.

2.6 Preparation of hydrogels for cell culture

Sheet-formed DN gel, PCDME gel, and PNaSS gel were punched into disks (35 mm in diameter and 1.2 mm thick) and autoclaved in HEPES buffer. The disk was transferred to a 35 mm polystyrene dish, and 2 mL of culture medium was added to each dish and

immersed overnight in a humid incubator at 37°C, 5% CO_2. The next day, remaining medium in the dishes was removed, and fresh medium containing cells was seeded on the gels.

2.7 Real-time polymerase chain reaction (PCR) analysis

Total RNA from cultured mesothelioma cells was extracted using the RNeasy Mini kit (Qiagen, Valencia, CA). The cDNA was synthesized using Superscript VILO (Thermo Fisher Scientific). Real-time PCR was performed by a step-one real-time PCR system (Applied Biosystems, Foster City, CA) using SYBR Green PCR Master Mix (Qiagen). Primer sequences are shown in **Supplementary Table 1**. Relative expression levels of genes of interest were normalized by the delta delta Ct method with *glyceraldehyde 3-phosphate dehydrogenase* (*GAPDH*) as the endogenous control.

2.8 Xenograft models and bioluminescense imaging

7-week-old female Balb/cA Jcl nu/nu nude mice (CLEA Japan, Inc.) were used. tdTomato-Luc2-transfected ACC-MESO-4 cells and MSTO-211H cells (1.0×10^5 cells/mL) were seeded on PS dish and PNaSS gel and cultured for 3 days. Thereafter, 5.0×10^4 ACC-MESO-4 and 1.0×10^3 MSTO-211H cells were suspended in 50 μL of medium and injected to the abdominal wall of mice (n=4/group). Mice were anesthetized with 1.75% isoflurane (60 mg/kg) inhalation. The abdominal midline of the mice was incised and the cell suspension was injected in a dome shape between the parietal peritoneum and muscle layer, and then the peritoneum and skin were carefully sutured. Bioluminescence imaging using the IVIS Spectrum imaging system (Summit Pharmaceuticals International Co., Tokyo, Japan) was performed after injection of

VivoGlo Luciferin, In Vivo Grade (Promega Co., Wisconsin, USA) into the abdominal cavity of the mice. All animal experiments were conducted in compliance with the guidelines of Hokkaido University Manual for Implementing Animal Experimentation with the approval of Institutional Animal Care and Use Committee at Hokkaido University Faculty of Medicine, Sapporo, Japan (Number 17–0061, 22-0089).

2.9 Microarray analysis and enrichment analysis

ACC-MESO-4 cells were cultured on DN gel, PS dish and ultra-low attachment (ULA) dish for 3 days. Total RNA of these cells was extracted using the RNeasy Mini kit (Qiagen). Microarray analysis was performed using SurePrint G3 Human Gene Expression 8× 60K v3.0 (Agilent Array). Data were standardized and analyzed using processes established in the Minimum Information About a Microarray Experiment (MIAME) guidelines. Gene expression levels were analyzed by comparing expression on DN gels with those on PS dishes and ULA dishes. 101 up-regulated genes with a Log2FC (fold change) greater than 0.6 were performed enrichment analysis using Enrichr, a comprehensive resource for curated gene sets (URL: https://maayanlab.cloud/Enrichr/). Microarray data set was uploaded to NCBI Gene Expression Omnibus (GEO) as accession number GSE286050.

2.10 Western blotting

ACC-MESO-4 cells were cultured on PS dish, DN gel, PCDME gel, and PNaSS gel for 3 days to prepare lysate samples. Lysate samples were also prepared from HEK293T cells transiently overexpressing SLC13A5 and its empty control. As lysis buffer, RIPA buffer prepared in our laboratory was used. The samples were resolved on SDS-

polyacrylamide gels (7-12%) and transferred to PVDF membranes by electrophoresis. The membranes were then incubated with primary antibody and horseradish peroxidase (HRP)-conjugated secondary antibody and developed using Cytiva Amersham™ ECL™ Western Blotting Detection Reagents (Leicestershire, England). Lumino image analyzers (ImageQuant LAS 4000mini system; GE Healthcare Japan, Co., Japan) were used for visual detection and analysis. Primary antibodies are anti-SOX2 antibody (#3579), anti-YAP/TAZ antibody (#8418), anti-phospho-YAP antibody (S127) (#13008), anti-ERK1/2 antibody (#9102), anti-phospho-ERK1/2 antibody (T202/Y204) (#9101), anti-mTOR antibody (#2983), anti-phospho-mTOR antibody (S2481) (#2974), anti-p53 antibody (#2524), anti-AMPK-alpha antibody (#5831), anti-phospho-AMPK-alpha antibody (T172) (#2535) (Cell Signaling Technology, Beverly, MA, USA), anti-Actin antibody (MAB1501, Millipore), anti-SLC13A5 antibody (sc-293277, Santa Cruz Biotechnology, Texas, USA), anti-TMEM151B antibody (MBS9204525, myBioSource), anti-HCRTR2 antibody (AOR-002, Alomone Labs Ltd., Jerusalem, Israel), and anti-FLAG M2 antibody-peroxidase (HRP)-conjugated antibody (A8592) (Sigma-Aldrich).

2.11 Immunostaining of SLC13A5 using cell block

ACC-MESO-4 cells cultured on PS dish, DN gel, PCDME gel, and PNaSS gel were detached with 0.25% trypsin-EDTA solution (Sigma-Aldrich), and centrifuged at 1,500 rpm for 3 minutes, and the resulting pellet was embedded in paraffin blocks. Immunostaining was performed using anti-SLC13A5 antibody (sc-293277, Santa Cruz Biotechnology). The staining process was performed according to the Envision FLEX visualization system (Dako; Agilent Technologies, Inc., California, USA).

2.12 Immunofluorescence

MSTO-211H cells and HEK293T cells transiently overexpressing SLC13A5 were cultured on a glass-based dish and immunofluorescence was performed using anti-Flag M2 antibody (F-3165, Sigma-Aldrich) as the primary antibody and Alexa Fluor 594-conjugated anti-mouse IgG antibody (A11032, Thermo Fisher Scientific) as the secondary antibody. The cells were observed using a confocal laser scanning microscope (FV3000; Olympus Co., Tokyo, Japan).

2.13 Metabolic analysis

HEK293T cells with SLC13A5 transient overexpression and its control cells were suspended in XF assay medium supplemented with 10 mM glucose, 1 mM pyruvate, and 2 mM glutamine. The cells (1×10^4 cells/well) were seeded into culture plates coated with Cell-Tak (Thermo Fisher Scientific). Plates were centrifuged and equilibrated in 37°C incubator for 45 min before transfer to Seahorse XFp extracellular flux analyzer (Agilent Technologies, Inc.). Oxygen consumption rate (OCR) was measured by the Mito Stress Test. First, basal respiration was measured in XF assay medium (1 mM sodium pyruvate, 10 mM glucose, 2 mM glutamine). Next, oligomycin (1 μM) was injected and respiration associated with ATP production was measured. In addition, the binding inhibitor carbonyl cyanide 4-(trifluoromethoxy)phenylhydrazone (FCCP, 1 μM) was added and maximal respiration was measured. Finally, rotenone and antimycin A (0.5 μM each) were added in combination, and non-mitochondrial respiration was measured.

2.14 CCK-8 assay

To examine the sensitivity to antitumor drug, the cell viability was evaluated by CCK-8 assay kit (FUJIFILM Wako Pure Chemical Co.). MSTO-211 H cells transiently overexpressing SLC13A5 and the control cells were seeded in 96 well plate at 1×10^4 cells/well. After 24 hours of incubation, cisplatin was administered at 0, 0.1, 1, 10, 50, and 100 μM. After additional 24 hours, CCK-8 assay was performed and absorbance at 450 nm was measured. The average viability was calculated using Excel by subtracting the blank value from the absorbance obtained [((control－sample)/control) ×100]. Data were plotted on a graph with the logarithm-transformed drug dose on the x-axis and the average viability on the y-axis. IC50 values were estimated using a fitted line [linear regression: Y = a × X + b, IC50 = (0.5 - b)/a].

2.15 Statistical Analysis

ImageJ-software (URL: https://imagej.net/software/fiji/) was used to measure spheroid morphology and to calculate the immunostaining positive area of cells. Graphical data were presented as means and standard deviations. Student's t-test was used for comparisons, and a P-value less than 0.05 was considered significant. The F-test was used to examine whether the samples were in equal or not equal variances.

2.16 Survival analysis using clinical database

Survival analyses were performed using two public datasets: the TCGA database from 87 patients using the online tool GEPIA [35] and the Bueno cohort from 211 patients [36]. pyEGA3 was used to download the raw files stored in the EGA database (EGAD00001001915), and after removing the adapters using Trim Galore v0.6.3, the

Fastq files were used with Salmon v1.10.1[37] to direct quantification (reference genome: GRCh38). Raw counts data were imported into the R environment (R 4.3) for subsequent analyses, data filtering and normalization were performed using the R package ‘DESeq2’ [38], and survival analyses were performed based on the R package ‘Survival’.

2.17 scRNA-seq data analysis of mesothelioma dataset

The public mesothelioma scRNA-seq dataset (GSE201925) were downloaded from Gene Expression Omnibus database [39]. The expression matrix (reference genome: GRCh38) was calculated using Cellranger 7.1.0 (10×Genomics). Subsequent analysis was performed mainly based on the R package 'Seurat v4' [40]. Cells were first undergoing quality control and only cells meeting the criteria were retained: genes (min: 300-max: 10000), mitochondrial gene percent (<20%), unique molecular identifiers count (<80,000). Genes expressed in no more than 3 cells were also removed. The R package 'Tricycle'[41] was used to infer the cell cycle situation to avoid the impact of cell cycle on the subsequent analysis. Afterwards, different samples were integrated using the CCA algorithm to remove batch effects.

The *FindVariableFeatures()* function was used to screen 3000 highly variable genes for PCA dimensionality reduction and clustering operations (PCs=1:40, Resolution=0.5), and all cells were divided into 15 clusters then used uniform manifold approximation and projection (UMP) algorithm for visualization. Then, the marker genes in each cluster were calculated by the *FindAllMarkers()* function and the cell types were manually annotated.

3. Results

3.1 Induction of mesothelioma stem cells by the DN hydrogel

On the basis of the novel technique we established, the hydrogel-activated reprogramming (HARP) phenomenon [23], five human mesothelioma cell lines (MSTO-211H, ACC-MESO-4, NCI-H2052, NCI-H2452, and NCI-H28) were cultured on PS dishes and DN gels for 24 hours. These cell lines adhered in a monolayer on the PS dishes, whereas they floated and formed spheroids on the DN gels (**Figure 1B**). MSTO-211H cells were tightly aggregated to form spheres, and other four cell lines formed loose aggregates with recognizable cell boundaries (**Figure 1B**). Although the size of spheroids appears to vary depending on the cells, the average short diameter of the top 10 spheroids ranged 80 to120 μm, with no significant differences (**Figure 1C**). The expression levels of pan-stem cell markers *SOX2*, *Nanog*, and *Oct3/4* were significantly greater in MSTO-211H, ACC-MESO-4 and NCI-H2452 cells cultured on DN gels than in those cultured on PS dishes, and this tendency was also observed in NCI-H2052 cells (**Figure 1D**). These results indicate that these four human mesothelioma cell lines respond favorably to DN gels, increasing their expression of stem cell markers.

3.2 HCRTR2, SLC13A5, and TMEM151B are upregulated and glycogenesis is promoted in DN gel-induced MesoSC-like cells

Since the effects of DN gel-induced stemness were more pronounced in ACC-MESO-4 cells (**Figure 1D**), we comprehensively investigated gene expression in ACC-MESO-4 cells cultured on the DN gel via microarray analysis. To identify novel mesothelioma stem cell markers that could serve as therapeutic targets, gene expression

on the DN gel was compared with that on control PS dishes as well as ultralow attachment (ULA) dishes, a classical method for enriching stem cells. Microarray analysis identified 23 genes as stem cell marker candidates whose expression was increased by more than 20-fold on the DN gel compared with that on the PS and ULA dishes, and 8 of these genes encoded membrane proteins that could be potential therapeutic targets (**Figure 2A**). Real-time PCR analysis revealed a common tendency toward increased expression of *HCRTR2*, *SLC13A5*, and *TMEM151B* in MSTO-211H, ACC-MESO-4 and NCI-H2452 cells cultured on DN gels (**Figure 2B**). Meanwhile, the other five genes were excluded from further investigation because four genes (*PLB1*, *RXFP1*, *SEMA4G* and *SLC6A11*) did not show increased expression in ACC-MES-4 cells on the DN gel (**Supplementary Figure 1A**), and *PTGFR* was not sufficiently expressed in other mesothelioma cell lines (**Supplementary Figure 1B**). Enrichment analysis via the Kyoto Encyclopedia of Genes and Genomes (KEGG) pathway database of 101 genes whose Log2FC was greater than 0.6 on DN gels compared with those on PS and ULA dishes revealed the upregulation of glycogenic amino acids such as histidine, tyrosine, and alanine, suggesting the promotion of the TCA cycle and gluconeogenesis (**Figure 2C**). Furthermore, the Molecular Signatures Database (MSigDB) pathway analysis revealed increased epithelial–mesenchymal transition (EMT) (**Supplementary Figure 2A**). Real-time PCR verified significantly increased expression of several EMT-related genes, such as *slug*, *fibronectin*, *twist*, and *N-cadherin,* in ACC-MESO-4 cells cultured on the DN gel compared with those cultured on the PS dish (**Supplementary Figure 2B**).

3.3 SLC13A5-, HCRTR2-, and TMEM151B-expressing cell clusters were identified in mesothelioma datasets

To examine the expression of *SLC13A5*, *TMEM151B*, and *HCRTR2* in human clinical mesothelioma samples, clustering was performed via the scRNA-seq gene expression dataset from Knelson et al [39]. By UMAP clustering, the tumor cells were broadly divided into two clusters (**Figure 2D**). Tumor Cluster 1 was separate from tumor Cluster 2, and Cluster 1 had higher expression of genes, including *CLDN15*, *CA9*, *HP*, *MST1*, and *RYR2* (marked with * in **Figure 2E**). Notably, tumor cells expressing *SLC13A5*, *TMEM151B*, *HCRTR2*, and the stemness markers *SOX2* and *Oct3/4* (*POU5F1*) belonged to Cluster 1 (marked with ** in **Figure 2E**). The expression levels of these genes were quite low but specific for tumor Cluster 1. These results are consistent with reports that mesothelioma contains a lower percentage of MesoSCs (0.27–1.32% of whole tumor cells) [42].

3.4 PNaSS gel-induced MesoSCs along with the induction of SLC13A5, HCRTR2, and TMEM151B

The HARP phenomenon can be observed not only in DN gels but also in certain types of single-network (SN) hydrogels, such as PCDME (poly(N-(carboxylmethyl)-N,N'-dimethyl-2-(methacryloyloxy)ethanaminium, inner salt) and PNaSS (sodium p-styrene sulfonate) gels (**Figure 3A**), which exhibit different properties from DN gels (**Supplementary Table 2)** [26–28]. Unlike on the DN gel, the ACC-MESO-4 cells did not form spheroids on the PCDME and PNaSS gels, and showed various morphologies such as elongated and polygonal shape (**Figure 3B**). Real-time PCR analysis revealed that for nine genes (*SOX2*, *Nanog*, *Oct4*, *CD44*, *ALDH1A2*, *ALDH1A3*, *CD9*, *CD24*,

and *CD26*) previously reported to be associated with MesoSCs [18–21], the expression of six genes (*SOX2*, *Nanog*, *Oct4*, *CD44*, *ALDH1A3*, and *CD9*) was significantly increased on all three hydrogels (**Figure 3C**). The expression levels of MesoSC marker candidate molecules, such as *HCRTR2*, *SLC13A5*, and *TMEM151B,* were also increased (**Figure 3C**). The analysis of the TCGA database revealed that although there was no significant difference in the Kaplan-Meier curve, patients with high expression of *HCRTR2, SLC13A5*, and *TMEM151B* genes tended to have a worse prognosis than those with low expression (**Supplementary Figure 3**).

3.5 Increased expression of SLC13A5 in hydrogel-induced MesoSC-like cells and enhanced tumorigenicity in vivo

To analyze the role of SLC13A5, Western blotting was performed, and we found that the expression level of SLC13A5 was increased in cells grown on the three types of hydrogels, being 4.7-, 4.6-, and 7.4-fold greater on DN, PCDME, and PNaSS gels, respectively, than in cells grown on PS dish (**Figure 3D**). Notably, examining the protein levels of TMEM151B and HCRTR2 was difficult because of the low specificity of the antibodies (data not shown). Immunostaining of the cell block samples revealed that the cells on the hydrogel highly expressed SLC13A5 not only on the cell membrane but also in the cytoplasm (**Figure 3E**), with the highest expression levels when grown on the PNaSS gels (**Figure 3F**).

We next examined tumorigenicity *in vivo* to investigate the stem cell properties of the cells cultured on the hydrogel. The PNaSS gel was selected because it induced the highest expression of SLC13A5 protein (**Figure 3D, 3F**). MSTO-211H cells with tdTomato-Luc2 expression were cultured on PS dishes and PNaSS gels and transplanted

into the mesothelial stroma just below the peritoneum of nude mice (n = 4/group). In 2/4 mice (50%, mice #1 and #2) in the PNaSS gel, enhanced luminescence was observed at 7 weeks compared with those in the PS group (0/4 mice, 0%) (P = 0.044037, **Figure 3G, 3H**). In the case of ACC-MESO-4 cells, two (50%) and three (75%) mice in the PS dish and PNaSS gel groups, respectively, presented increased luminescence at 5 weeks (P = 0.626937, **Supplementary Figure 4**). These results suggest that the properties of the cells changed, and the cells acquired stemness through hydrogel culture. SLC13A5 may play an important role in reprogramming into MesoSC-like cells.

3.6 SLC13A5 overexpression induces metabolic shifts to oxidative phosphorylation (OXPHOS) and cisplatin resistance

To investigate the functional signature of SLC13A5 in living cells, SLC13A5 was transiently overexpressed in several cell lines. ACC-MESO-4 and MSTO-211H cells presented low transfection efficiencies of less than 5% and 30-40%, respectively (**Supplementary Figure 5**). HEK293T cells were also used because of their high transfection efficiency and lack of endogenous expression of SLC13A5 (**Figure 4A**). FLAG-tagged SLC13A5 was localized on the plasma membrane of MSTO-211H and HEK293T cells (**Figure 4B,** red color).

Since SLC13A5 is involved in the TCA cycle as a citrate transporter [43, 44], we first focused on cellular energy metabolism. Using a mitochondrial stress test to measure the oxygen consumption rate (OCR), we found that basal and maximal respiratory activities were significantly increased in SLC13A5-overexpressing cells, which indicates that energy production was shifted to oxidative phosphorylation

(OXPHOS) (**Figure 4C**). Western blotting revealed that in stemness-related signaling pathways, the phosphorylation levels of YAP and ERK1/2 were increased in SLC13A5-overexpressing cells, as was the expression of SOX2 (**Figure 4D**), which is consistent with the acquisition of stemness.

Furthermore, a CCK-8 assay was performed using SLC13A5-overexpressing MSTO-211H cells to examine the role of SLC13A5 in resistance to cisplatin. Compared with control cells, cells overexpressing exogenous SLC13A5 presented higher IC50 values and resistance to cisplatin (IC50 values = 24.0 μM and 14.0 μM for SLC13A5-overexpressing and control cells, respectively). In the presence of 1 μM cisplatin, the viability of SLC13A5-overexpressing cells was significantly increased ($P = 0.031283$, **Figure 4E**). These results suggest that SLC13A5 contributes to efficient energy metabolism and drug resistance in MesoSCs, suggesting its usefulness as a potential therapeutic target and diagnostic marker.

Discussion

The purpose of this study was to clarify whether our previously developed hydrogel-based CSC induction method, termed the hydrogel-activated reprogramming (HARP) phenomenon, can be applied to human mesothelioma cell lines. We analyzed the characteristics of the resulting mesothelioma stem cells (MesoSCs) and identified molecules essential for the development of novel MesoSC-targeting therapies. According to reports using conventional MesoSC extraction methods, MesoSCs are identified as cells that fulfill two or more of the following characteristics: spheroid formation, Matrigel invasion, migration, tumorigenesis, angiogenesis, EMT, and high

expression of pan-stem cell markers [16–21, 31]. Notably, in the case of mesothelial cells, the EMT phenomenon is called MMT (mesothelial–mesenchymal transition). In this study, we demonstrated that ACC-MESO-4, MSTO-211H, and NCI-H2452 cells cultured on DN gels exhibited spheroid formation and increased expression of pan-stem cell markers (*SOX2*, *Nanog*, and *Oct3/4*) (**Figure 1B, 1D**). ACC-MESO-4 cells also exhibited increased EMT/MMT (**Supplementary Figure 2A, 2B**) and increased expression of pan-stem cell markers and MesoSC-associated genes on PCDME and PNaSS gels (**Figure 2F**). Furthermore, MSTO-211H cells cultured on PNaSS gel had an advantage in terms of tumorigenicity (**Figure 3G, 3H**). These results confirmed that the characteristics of the human mesothelioma cell lines acquired via the hydrogel culture method were quite similar to those of MesoSCs.

Although elucidating the molecular mechanisms of MesoSC induction on the three types of hydrogels remains a challenge, we speculate that differences in the charge and elasticity of the gel mimics different tumor microenvironments, potentially reprogramming mesothelioma into MesoSCs [45]. This method has clear advantages over conventional methods in terms of simplicity because of the short culture period and the lack of expensive reagents and equipment. Furthermore, the identification of SLC13A5 as a novel MesoSC marker in this study suggests that the use of hydrogel may be valuable for characterizing MesoSCs and identifying therapeutic targets.

Here, we demonstrated that SLC13A5 expression was increased at both the gene and protein levels in hydrogel-induced MesoSC-like cells (**Figure 2B, 3A**). SLC13A5 has been reported to encode a transmembrane protein, the sodium-dependent citrate transporter (NaCT) [43, 44]. On the other hand, immunostaining revealed that SLC13A5/NaCT in the MesoSC-like cells was localized not only on the plasma

membrane but also in the cytoplasm (**Figure 3E**). It is possible that NaCT is internalized into the cytoplasm or may be transported followed by rapid turnover. At present, little is known about the mechanism of the translational regulation of NaCT, and further analysis is needed [46]. According to the Western blotting (**Figure 3D**) and the databases of The Human Protein Atlas (URL: https://www.proteinatlas.org/) and DISCO (URL: https://www.immunesinglecell.org/), endogenous expression of SLC13A5 was not detected or was negligible in existing mesothelial cells and mesothelioma cell lines. This means that the increased expression in MesoSC-like cells may play an important role even at a low level; therefore, we performed an overexpression analysis to analyze the function of SLC13A5/NaCT in MesoSC-like cells.

Mito stress tests demonstrated that high SLC13A5 expression significantly increased basal and maximal respiratory activity and shifted cellular metabolism toward OXPHOS (**Figure 4C**). Recently, several types of CSCs were reported to use OXPHOS-dependent energy metabolism[47, 48], which suggests that SLC13A5 increases the energy production capacity of cancer cells, increasing their energy metabolism closer to that of CSCs. Furthermore, SLC13A5-overexpressing cells presented increased SOX2 expression and increased phosphorylation of ERK1/2 and YAP (**Figure 4D**). In gastric cancer and lung cancer, activation of ERK-SOX2 signaling has been reported to promote stemness and metastasis [49, 50]. ERK activation has also been reported to lead to YAP activation and cell proliferation in breast cancer [51]. Therefore, ERK-SOX2 and ERK-YAP signaling may be activated in MesoSCs. The AKT pathway contributes to mesothelioma progression and cell migration [52–54]. In liver cancer, knockdown of SLC13A5 to reduce citrate influx has been reported to

relieve AMPK inhibition and decrease cell proliferation *via* mTOR signaling [55], but there was no change in the phosphorylation levels of AMPK or mTOR (**Figure 4D**). These findings suggest that SLC13A5 may activate ERK1/2 through an unknown interaction, which requires further analysis in the future.

Analysis of cytotoxicity via a CCK-8 assay revealed that high SLC13A5 expression led to the acquisition of cisplatin resistance (**Figure 4E**). Citrate is a component of the TCA cycle and plays important roles in energy production by inhibiting the rate-limiting enzymes of glycolysis and promoting lipid synthesis and gluconeogenesis [56, 57]. NaCT-mediated citrate uptake has also been reported to be metabolically important under nutrient-limited conditions and may promote resistance to metal toxicity [58]. Our enrichment analysis revealed increased glycogen amino acid metabolism (**Figure 2C**), suggesting that MesoSC-like cells have increased gluconeogenesis and are in a state close to undernutrition. Thus, the present study demonstrated that SLC13A5/NaCT might metabolically contribute to the survival of MesoSCs. The application of ion channels has been reported in breast cancer stem cells with features of drug-tolerant persisters [59].

Although we evaluated the mRNA expression of *SLC13A5* and stem cell markers that characterize MesoSC-like cells in clinical samples via scRNA-seq database analysis (**Figure 2D**), there is currently only one report that used an open access database; thus, it is desirable to accumulate more cases in the future. In addition, knockdown or knockout experiments would be ideal to identify the function/mechanism of SLC13A5. However, this was difficult to perform because endogenous expression of SLC13A5 in mesothelioma cells was almost non-existent, and it was also not enough for knockdown in hydrogel-induced MesoSC-like cells. Even with these limitations, this study is

valuable because it is the first to identify SLC13A5 as a key molecule contributing to MesoSC survival *via* the hydrogel-activated reprogramming phenomenon.

Conclusion

Our hydrogel-based culture method involving the HARP phenomenon successfully induced MesoSCs from several human mesothelioma cell lines. We also identified *SLC13A5*, *TMEM151B,* and *HCRTR2* as novel genes that are specifically expressed in MesoSCs. Among them, SLC13A5 shifts cellular energy metabolism to OXPHOS and contributes to the acquisition of drug resistance. Taken together, these findings suggest that SLC13A5 might be useful as a novel MesoSC marker and therapeutic target for eradicating mesothelioma.

Conflicts of interest

Shinya Tanaka and Mishie Tanino are the Editor-in-Chief and Editorial Board members, respectively, of Pathology International and co-author of this article. To minimize bias, they were excluded from all editorial decision-making related to the acceptance of this article for publication.

Ethics Approval statement

All animal experiments were conducted in compliance with the guidelines of Hokkaido University Manual for Implementing Animal Experimentation with the approval of Institutional Animal Care and Use Committee at Hokkaido University Faculty of Medicine, Sapporo, Japan (Number 17–0061, 22-0089). For human subjects, the investigation was conducted in accordance with the Declaration of Helsinki of 1975. In

this study, publicly available datasets were utilized for the analyses; the TCGA database and Bueno cohort for survival analyses and the mesothelioma scRNA-seq dataset (GSE201925) from Gene Expression Omnibus database.

Authors' contributions

Marie Kato-Shinomiya and Hirokazu Sugino performed the experiments, and Yusuke Saito, Jintao He, Zen-ichi Tanei, and Yoshitaka Oda analyzed the data. Jian Ping Gong synthesized the hydrogels. Masumi Tsuda and Shinya Tanaka designed the study, revised the manuscript, and approved the final version for publication. Satoshi Tanikawa, Lei Wang, and Mishie Tanino assisted with the study design. All of the authors read and approved the manuscript.

Acknowledgments

This research was financially supported by the Japan Society for the Promotion of Science (JSPS, Grant Numbers JP21K08196, HS; JP19H01171 and JP24H00037, ST; JP21H03802 and JP24K03245, MT).

Reference

1. Yates DH, Corrin B, Stidolph PN, Browne K. Malignant mesothelioma in south east England: clinicopathological experience of 272 cases. Thorax. 1997;52:507–12.
2. Walpole S, Pritchard AL, Cebulla CM, Pilarski R, Stautberg M, Davidorf FH, et al. Comprehensive study of the clinical phenotype of germline BAP1 variant-carrying families worldwide. Journal of the National Cancer Institute. 2018;110:1328–41.
3. Scherpereel A, Astoul P, Baas P, Berghmans T, Clayson H, De Vuyst P, et al. Guidelines of the European Respiratory Society and the European Society of Thoracic Surgeons for the management of malignant pleural mesothelioma. European Respiratory Journal. 2010;35:479–95.
4. Price B. Projection of future numbers of mesothelioma cases in the US and the increasing prevalence of background cases: an update based on SEER data for 1975 through 2018. Critical

Reviews in Toxicology. 2022;52:317–24.
5. Han Y, Zhang T, Chen H, Yang X. Global magnitude and temporal trend of mesothelioma burden along with the contribution of occupational asbestos exposure in 204 countries and territories from 1990 to 2019: Results from the Global Burden of Disease Study 2019. Critical Reviews in Oncology/Hematology. 2022;179:103821.
6. Baldini EH, Richards WG, Gill RR, Goodman BM, Winfrey OK, Eisen HM, et al. Updated patterns of failure after multimodality therapy for malignant pleural mesothelioma. Journal of Thoracic and Cardiovascular Surgery. 2015;149:1374–81.
7. Van Meerbeeck JP, Scherpereel A, Surmont VF, Baas P. Malignant pleural mesothelioma: The standard of care and challenges for future management. Critical Reviews in Oncology/Hematology. 2011;78:92–111.
8. Nakagawa K, Yamazaki K, Kunitoh H, Hida T, Gemba K, Shinkai T, et al. Efficacy and safety of pemetrexed in combination with cisplatin for malignant pleural mesothelioma: A phase I/II study in Japanese patients. Jpn J Clin Oncol. 2008;38:339–46.
9. Schumann SO, Kocher G, Minervini F. Epidemiology, diagnosis and treatment of the malignant pleural mesothelioma, a narrative review of literature. Journal of Thoracic Disease. 2021;13:2510–23.
10. Tagliamento M, Bironzo P, Curcio H, De Luca E, Pignataro D, Rapetti SG, et al. A systematic review and meta-analysis of trials assessing PD-1/PD-L1 immune checkpoint inhibitors activity in pre-treated advanced stage malignant mesothelioma. Critical Reviews in Oncology/Hematology. 2022;172.
11. Cornedine J. de Gooijer, Frank J. Borm, Arnaud Scherpereel, Paul Baas. Immunotherapy in Malignant Pleural Mesothelioma. Frontiers in Oncology. 2020;10.
12. Hu ZI, Ghafoor A, Sengupta M, Hassan R. Malignant mesothelioma: Advances in immune checkpoint inhibitor and mesothelin-targeted therapies. Cancer. 2021;127:1010–20.
13. Valent P, Bonnet D, De Maria R, Lapidot T, Copland M, Melo J V., et al. Cancer stem cell definitions and terminology: The devil is in the details. Nature Reviews Cancer. 2012;12:767–75.
14. Li F, Tiede B, Massagué J, Kang Y. Beyond tumorigenesis: Cancer stem cells in metastasis. Cell Research. 2007;17:3–14.
15. Dean M, Fojo T, Bates S. Tumour stem cells and drug resistance. Nature Reviews Cancer. 2005;5:275–84.
16. Hotta A, Cheung AYL, Farra N, Garcha K, Chang WY, Pasceri P, et al. EOS lentiviral vector selection system for human induced pluripotent stem cells. Nat Protoc. 2009;4:1828–44.
17. Blum W, Pecze L, Felley-Bosco E, Wu L, de Perrot M, Schwaller B. Stem Cell Factor-Based Identification and Functional Properties of In Vitro-Selected Subpopulations of Malignant Mesothelioma Cells. Stem Cell Reports. 2017;8:1005–17.

18. Ghani FI, Yamazaki H, Iwata S, Okamoto T, Aoe K, Okabe K, et al. Identification of cancer stem cell markers in human malignant mesothelioma cells. Biochem Biophys Res Commun. 2011;404:735–42.
19. Varghese S, Whipple R, Martin SS, Alexander HR. Multipotent Cancer Stem Cells Derived from Human Malignant Peritoneal Mesothelioma Promote Tumorigenesis. PLoS One. 2012;7.
20. Yamazaki H, Naito M, Ghani FI, Dang NH, Iwata S, Morimoto C. Characterization of cancer stem cell properties of CD24 and CD26-positive human malignant mesothelioma cells. Biochem Biophys Res Commun. 2012;419:529–36.
21. Cortes-Dericks L, Froment L, Boesch R, Schmid RA, Karoubi G. Cisplatin-resistant cells in malignant pleural mesothelioma cell lines show ALDHhighCD44+ phenotype and sphere-forming capacity. BMC Cancer. 2014;14:304.
22. Chew S, Okazaki Y, Akatsuka S, Wang S, Jiang L, Ohara Y, et al. Rheostatic CD44 isoform expression and its association with oxidative stress in human malignant mesothelioma. Free Radic. Biol. Med. 2017;106:91-99.
23. Suzuka J, Tsuda M, Wang L, Kohsaka S, Kishida K, Semba S, et al. Rapid reprogramming of tumour cells into cancer stem cells on double-network hydrogels. Nat Biomed Eng. 2021;5:914–25.
24. Gong JP, Katsuyama Y, Kurokawa T, Osada Y. Double-network hydrogels with extremely high mechanical strength. Advanced Materials. 2003;15:1155–8.
25. Haas F, Volz J, Gehr R, Reichel J, Estève J. Entangled states of more than 40 atoms in an optical fiber cavity. Science (1979). 2014;344:180–3.
26. Yin H, Akasaki T, Lin Sun T, Nakajima T, Kurokawa T, Nonoyama T, et al. Double network hydrogels from polyzwitterions: High mechanical strength and excellent anti-biofouling properties. J Mater Chem B. 2013;1:3685–93.
27. Kaneko T, Mikoya T. Application of poly CDME (PCDME) gel to the palatal plate. Hokkaido J Dent Sci. 2017;38:136–9.
28. Yang JJ, Chen YM, Kurokawa T, Gong JP, Onodera S, Yasuda K. Gene expression, glycocalyx assay, and surface properties of human endothelial cells cultured on hydrogel matrix with sulfonic moiety: Effect of elasticity of hydrogel. J Biomed Mater Res A. 2010;95 A:531–42.
29. Prummel KD, Nieuwenhuize S, Mosimann C. The lateral plate mesoderm. Development . 2020;147.
30. Thomason RT, Bader DM, Winters NI. Comprehensive timeline of mesodermal development in the quail small intestine. Developmental Dynamics. 2012;241:1678–94.
31. Kandasamy S, Adhikary G, Rorke EA, Friedberg JS, Mickle MB, Alexander HR, et al. The YAP1 signaling inhibitors, verteporfin and CA3, suppress the mesothelioma cancer stem cell phenotype. Molecular Cancer Research. 2020;18:343–51.

32. Rina Ohashi, Ken Tajima, Fumiyuki Takahashi, Ri Cui, Tao Gu, Kazue Shimizu, et al. Osteopontin modulates malignant pleural mesothelioma cell functions in vitro. Anticancer Res. 2009;29:2205–14.
33. Tajima K, Ohashi R, Sekido Y, Hida T, Nara T, Hashimoto M, et al. Osteopontin-mediated enhanced hyaluronan binding induces multidrug resistance in mesothelioma cells. Oncogene. 2010;29:1941–51.
34. Usami N, Fukui T, Kondo M, Taniguchi T, Yokoyama T, Mori S, et al. Establishment and characterization of four malignant pleural mesothelioma cell lines from Japanese patients. Cancer Sci. 2006;97:387–94.
35. Tang Z, Li C, Kang B, Gao G, Li C, Zhang Z. GEPIA: A web server for cancer and normal gene expression profiling and interactive analyses. Nucleic Acids Res. 2017;45:W98–102.
36. Bueno R, Stawiski EW, Goldstein LD, Durinck S, De Rienzo A, Modrusan Z, et al. Comprehensive genomic analysis of malignant pleural mesothelioma identifies recurrent mutations, gene fusions and splicing alterations. Nat Genet. 2016;48:407–16.
37. Patro R, Duggal G, Love MI, Irizarry RA, Kingsford C. Salmon provides fast and bias-aware quantification of transcript expression. Nat Methods. 2017;14:417–9.
38. Love MI, Huber W, Anders S. Moderated estimation of fold change and dispersion for RNA-seq data with DESeq2. Genome Biol. 2014;15.
39. Knelson EH, Ivanova E V., Tarannum M, Campisi M, Lizotte PH, Booker MA, et al. Activation of Tumor-Cell STING Primes NK-Cell Therapy. Cancer Immunol Res. 2022;10:947–61.
40. Hao Y, Hao S, Andersen-Nissen E, Mauck WM, Zheng S, Butler A, et al. Integrated analysis of multimodal single-cell data. Cell. 2021;184:3573-3587.e29.
41. Zheng SC, Stein-O'Brien G, Augustin JJ, Slosberg J, Carosso GA, Winer B, et al. Universal prediction of cell-cycle position using transfer learning. Genome Biol. 2022;23.
42. Kai K, D'Costa S, Yoon B Il, Brody AR, Sills RC, Kim Y. Characterization of side population cells in human malignant mesothelioma cell lines. Lung Cancer. 2010;70:146–51.
43. Inoue K, Zhuang L, Ganapathy V. Human Na +-coupled citrate transporter: primary structure, genomic organization, and transport function. Biochem Biophys Res Commun. 2002;299:465–71.
44. Inoue K, Zhuang L, Maddox DM, Smith SB, Ganapathy V. Structure, function, and expression pattern of a novel sodium-coupled citrate transporter (NaCT) cloned from mammalian brain. Journal of Biological Chemistry. 2002;277:39469–76.
45. Prasetyanti PR, Medema JP. Intra-tumor heterogeneity from a cancer stem cell perspective. Molecular Cancer. 2017;16.
46. Bergeron MJ, Clémençon B, Hediger MA, Markovich D. SLC13 family of Na+-coupled di- and tri-carboxylate/sulfate transporters. Molecular Aspects of Medicine. 2013;34:299–312.
47. Sancho P, Barneda D, Heeschen C. Hallmarks of cancer stem cell metabolism. British Journal of

Cancer. 2016;114:1305–12.
48. Jones CL, Inguva A, Jordan CT. Targeting Energy Metabolism in Cancer Stem Cells: Progress and Challenges in Leukemia and Solid Tumors. Cell Stem Cell. 2021;28:378–93.
49. Lu J, Bang H, Kim SM, Cho SJ, Ashktorab H, Smoot DT, et al. Lymphatic metastasis-related TBL1XR1 enhances stemness and metastasis in gastric cancer stem-like cells by activating ERK1/2-SOX2 signaling. Oncogene. 2021;40:922–36.
50. Wang K, Ji W, Yu Y, Li Z, Niu X, Xia W, et al. FGFR1-ERK1/2-SOX2 axis promotes cell proliferation, epithelial–mesenchymal transition, and metastasis in FGFR1-amplified lung cancer. Oncogene. 2018;37:5340–54.
51. Qin X, Li J, Sun J, Liu L, Chen D, Liu Y. Low shear stress induces ERK nuclear localization and YAP activation to control the proliferation of breast cancer cells. Biochem Biophys Res Commun. 2019;510:219–23.
52. Rose AH, Bertino P, Hoffmann FW, Gaudino G, Carbone M, Hoffmann PR. Increasing dietary selenium elevates reducing capacity and ERK activation associated with accelerated progression of select mesothelioma tumors. American Journal of Pathology. 2014;184:1041–9.
53. Tamminen JA, Yin M, Rönty M, Sutinen E, Pasternack A, Ritvos O, et al. Overexpression of activin-A and -B in malignant mesothelioma - Attenuated Smad3 signaling responses and ERK activation promote cell migration and invasive growth. Exp Cell Res. 2015;332:102–15.
54. Li C, Rezov V, Joensuu E, Vartiainen V, Rönty M, Yin M, et al. Pirfenidone decreases mesothelioma cell proliferation and migration via inhibition of ERK and AKT and regulates mesothelioma tumor microenvironment in vivo. Sci Rep. 2018;8.
55. Kopel J, Higuchi K, Ristic B, Sato T, Ramachandran S, Ganapathy V. The Hepatic Plasma Membrane Citrate Transporter NaCT (SLC13A5) as a Molecular Target for Metformin. Sci Rep. 2020;10:8536.
56. Icard P, Poulain L, Lincet H. Understanding the central role of citrate in the metabolism of cancer cells. Biochimica et Biophysica Acta - Reviews on Cancer. 2012;1825:111–6.
57. Iacobazzi V, Infantino V. Citrate-new functions for an old metabolite. Biol Chem. 2014;395:387–99.
58. Avi Kumar, Thekla Cordes, Anna E. Thalacker-Mercer, Ana M. Pajor, Anne N. Murphy, Christian M. Metallo. NaCT/SLC13A5 facilitates citrate import and metabolism under nutrient-limited conditions. Cell Rep. 2021;36:109701.
59. Li M, Nishimura T, Takeuchi Y, Hongu T, Wang Y, Shiokawa D, et al. FXYD3 functionally demarcates an ancestral breast cancer stem cell subpopulation with features of drug-tolerant persisters. Journal of Clinical Investigation. 2023;133.

Figure legends

Figure 1. Induction of mesothelioma stem cell-like cells by DN gel

(A) Chemical structures of the components of the DN gel. The PAMPS as the first network gel (left) and PDMAAm as the second network gel (right) are shown. (B) Microscopy images of five mesothelioma cell lines, MSTO-211H (211H), ACC-MESO-4 (MESO-4), NCI-H2052 (H2052), NCI-H2452 (H2452), and NCI-H28 (H28), cultured on PS dishes (left) and on the DN gels (right). These cells adhered in a monolayer on the PS dishes, whereas they floated and formed spheroids on the DN gels. Scale bars: 50 μm. (C) Box-and-whisker plots show the short diameter of the top 10 spheroids formed on the DN gel derived from five mesothelioma cell lines (211H, MESO-4, H2052, H2452, and H28 cells), which were measured using Image J-software. The largest top 10 short diameters for each cell lines ranged 80 to 120 μm. The circle only in the box plot of 211H cells indicates an outlier, indicating that particularly large spheroid was formed. There were no such outliers in the other four cell lines. The × and bar in the box indicate the average and median, respectively. (D) Relative mRNA expression levels of pan-stem cell marker genes (*SOX2*, *Nanog*, and *Oct3/4*) in mesothelioma cell lines cultured on DN gels, showing significantly higher in 211H, MESO-4, and H2452 cells on the DN gel. *: $P < 0.05$, **: $P < 0.01$, ***: $P < 0.005$, and ******: $P < 0.0001$.

Figure 2. Upregulated genes in hydrogel-induced mesothelioma stem cell (MesoSC)-like cells and their clinical relevance.

(A) Microarray analysis of ACC-MESO-4 cells cultured on PS dish, ultra-low attachment (ULA) dish, and DN gel. Among the 23 genes whose expression increased more than 20-fold on the DN gel compared with the PS and ULA dishes, 8 genes encoding membrane proteins are shown in the table on the right. (B) Relative mRNA expression levels of HCRTR2, SLC13A5, and TMEM151B in five mesothelioma cell lines cultured on DN gel, showing significantly greater in MSTO-211H, ACC-MESO-4 and NCI-H2452 cells. Culture on PS dish was used as a control. *: $P < 0.05$, ***: $P < 0.005$, and ****: $P < 0.001$. (C) KEGG pathway enrichment analysis of upregulated genes in ACC-MESO-4 cells on the DN gel. The metabolism of glycogenic amino acids through the TCA cycle is increased. (D) Expression of candidate molecules that act as MesoSC markers (HCRTR2, SLC13A5, and TMEM151B) in clinical mesothelioma samples. Uniform manifold approximation and projection (UMAP) of cells in the mesothelioma scRNA-seq dataset (GSE 201925), color-coded with cell type annotation. (E) Marker genes expressed in each cluster. SLC13A5, TMEM 151B, HCRTR2, SOX2, and POUF1 (Oct 4) are expressed in tumor Cluster 1 of mesothelioma cells.

Figure 3. Protein expression analysis of SLC13A5 and evaluation of *in vivo* tumorigenicity in hydrogel-induced mesothelioma stem cell (MesoSC)-like cells.
(A) Chemical structures of the PCDME and PNaSS gel. (B) Microscopy images of ACC-MESO-4 cells cultured on PS dish, DN gel, PCDME gel, and PNaSS gel. They adhered firmly on PS dish, PCDME gel and PNaSS gel and floated spheroidal on DN gel. The scale bar is 100 μm. (C) Relative mRNA expression levels of candidate genes *HCRTR2*, *SLC13A5*, and *TMEM151B;* pan-stem cell marker genes such as *SOX2*, *Oct3/4*, and *Nanog*; and MesoSC-related genes such as *CD44*, *ALDH1A2*, *ALDH1A3*, *CD9*, *CD24*, and *CD26* in ACC-MESO-4 cells cultured on DN gel, PCDME gel, and PNaSS gel. *HCRTR2*, *SLC13A5*, *TMEM151B, SOX2*, *Nanog*, *Oct4*, *CD44*, *ALDH1A3*, and *CD9* were significantly increased on all three hydrogels. Culture on PS dishes was used as a control. *: $P < 0.05$, **: $P < 0.01$, ***: $P < 0.005$, ****: $P < 0.001$, *****: $P < 0.0005$, and ******: $P < 0.0001$. (D) Western blotting of SLC13A5 protein in ACC-MESO-4 cells cultured on PS dish, DN gel, PCDME gel, and PNaSS gel. SLC13A5 was 4.7-, 4.6-, and 7.4-fold greater on DN, PCDME, and PNaSS gels than on PS dish, respectively. Actin was used as a loading control. (E) Immunocytochemistry of SLC13A5 in ACC-MESO-4 cells cultured on PS dish, DN gel, PCDME gel, and PNaSS gel. H&E staining (upper panels) and SLC13A5 staining (lower panels) are shown. SLC13A5 was positive in the plasma membrane and cytoplasm. Scale bars: 25 μm. (F) In immunocytochemistry (E), the positive area of SLC13A5 staining in ACC-MESO-4 cells was significantly increased on PNaSS gel. *: $P < 0.05$, *****: $P< 0.0005$. (G) Images of tumors formed in the peritoneal cavity of mice visualized by the IVIS imaging system. The color scale for total photon counts ranges from 2000 (blue) to 5000 (red). (H) Evaluation of the *in vivo* tumorigenicity of MSTO-211H cells precultured on PS dish and PNaSS gel. The total photon counts of tumor cells were significantly evaluated 7 weeks after cell implantation. *: $P < 0.05$.

Figure 4. Effects of SLC13A5 on metabolism, cellular signaling, and drug resistance.
(A) The expression level of FLAG-tagged SLC13A5 transiently overexpressed in HEK293T cells was examined by Western blotting. Actin was used as a loading control. (B) Immunofluorescence of MSTO-211H (left) and HEK293T (right) cells transiently overexpressing FLAG-SLC13A5. FLAG-SLC13A5 and actin are visualized in green and red, respectively. FLAG-SLC13A5 was positive in the plasma membrane. The scale bars indicate 20 μm. (C) Mito stress test using HEK293T cells transiently

overexpressing SLC13A5 and control cells. The basal respiration rate (left), maximal respiration rate (middle), and basal OCR/ECAR ratio (right) were significantly increased in the overexpressing strain. *: $P < 0.05$. (D) The expression and phosphorylation levels of the indicated proteins in HEK293T cells transiently overexpressing SLC13A5 and control cells were examined by Western blotting. Actin was used as a loading control. SOX2 was clearly upregulated, and the phosphorylation levels of YAP and ERK1/2 were also increased as shown graphically (right). (E) MSTO-211H cells with or without exogenous SLC13A5 expression were treated with 1 μM cisplatin for 24 hours. The cell viability of overexpressing strain was significantly increased. *: $P < 0.05$.

Fig. 1

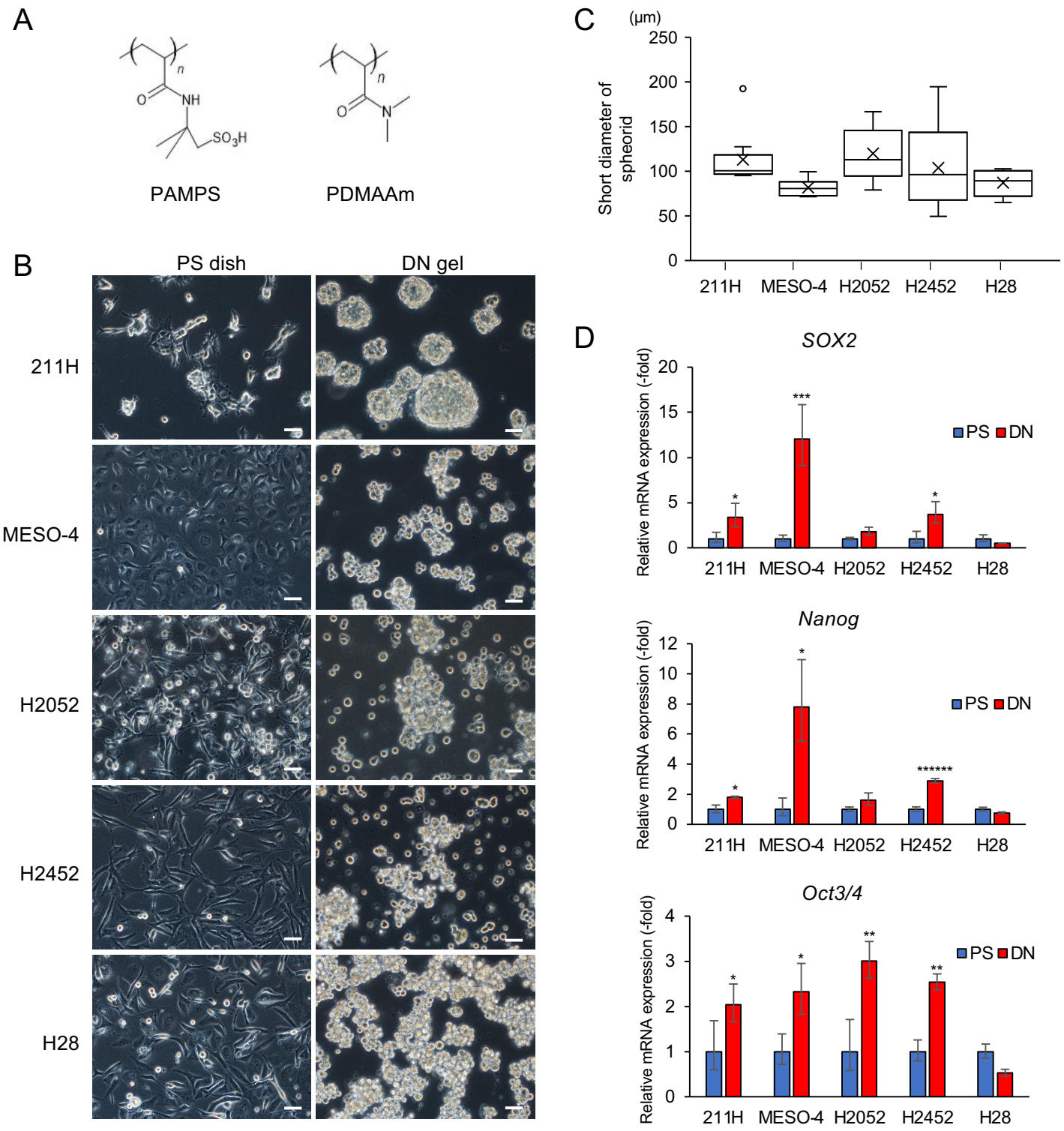
A
PAMPS
PDMAAm
B
PS dish
DN gel
211H
MESO-4
H2052
H2452
H28
C
(μm)
Short diameter of spheroid
250
200
150
100
50
0
211H
MESO-4
H2052
H2452
H28
D
SOX2
Nanog
Oct3/4
Relative mRNA expression (-fold)
PS
DN
211H
MESO-4
H2052
H2452
H28

Fig. 2

A

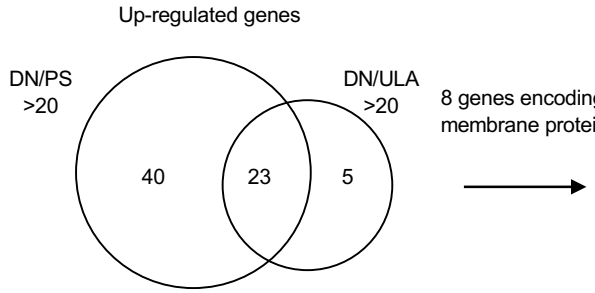

	Official Full Name
HCRTR2	Hypocretin receptor 2
PLB1	Phospholipase B1
PTGFR	Prostaglandin F receptor
RXFP1	Relaxin/insulin like family peptide receptor 1
SEMA4G	Semaphorin 4G
SLC13A5	Solute carrier family 13 member 5
SLC6A11	Solute carrier family 6 member 11
TMEM151B	Transmembrane protein 151B

B

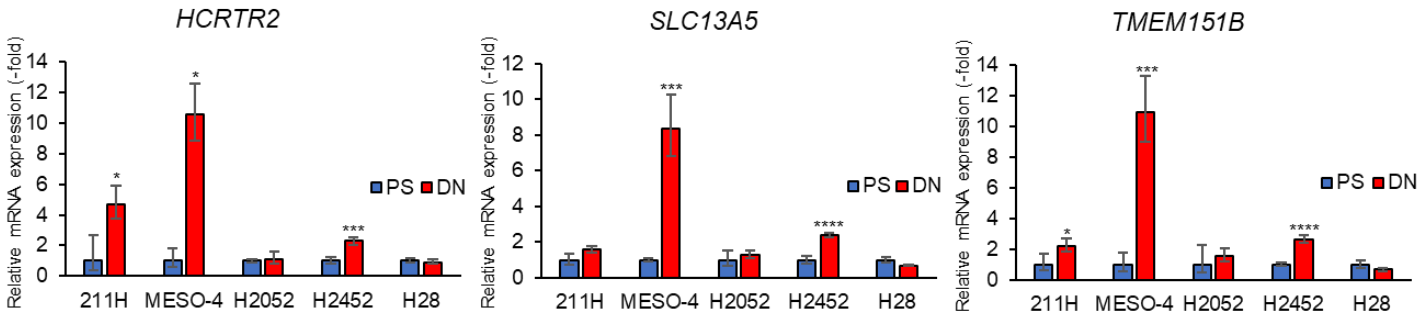

C

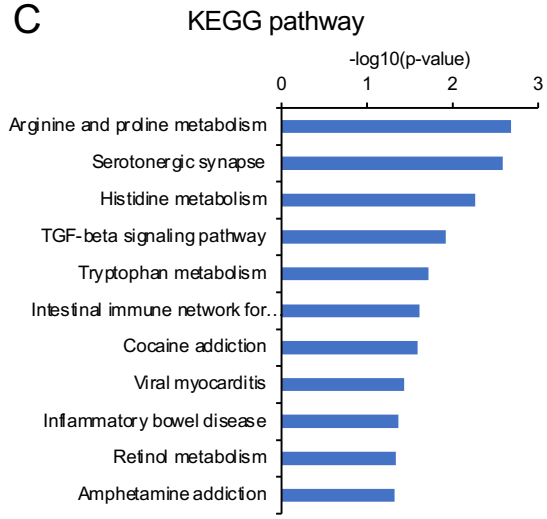

D

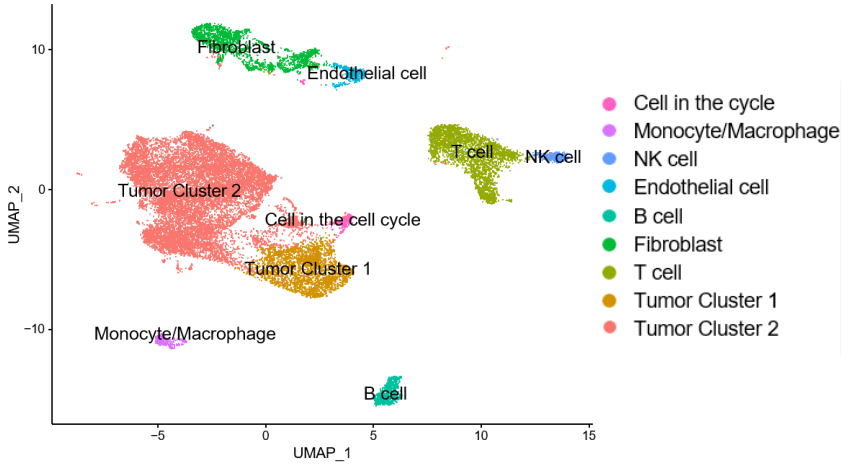

E

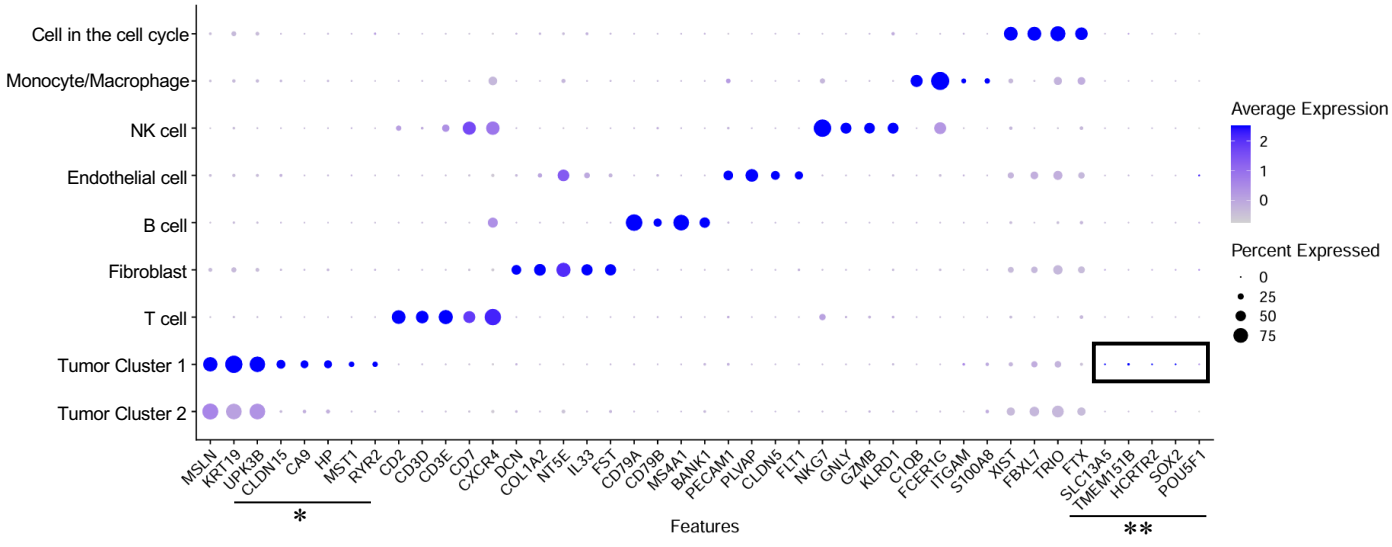

Fig. 3

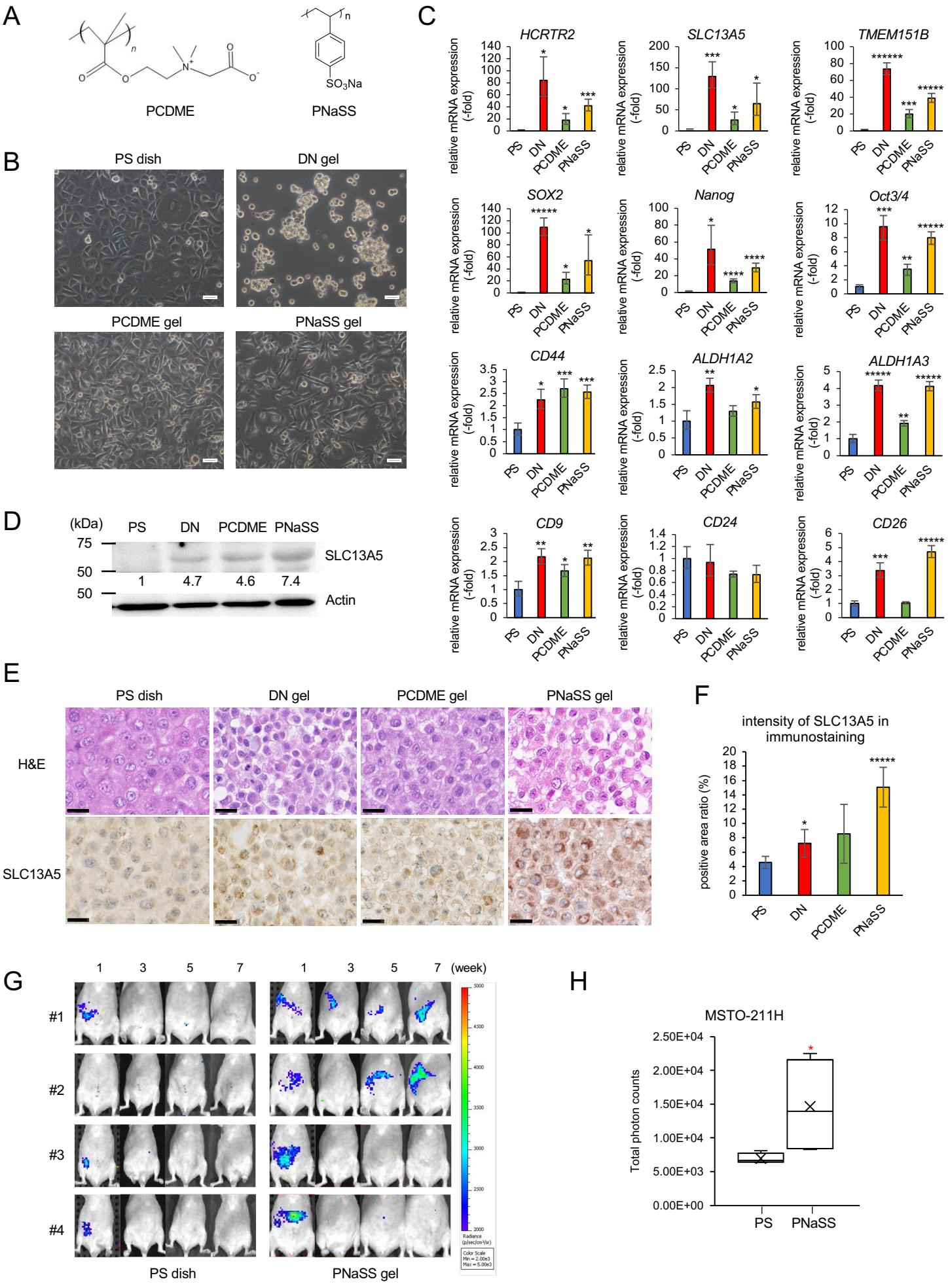
A
PCDME
PNaSS
B
PS dish
DN gel
PCDME gel
PNaSS gel
C
HCRTR2
SLC13A5
TMEM151B
SOX2
Nanog
Oct3/4
CD44
ALDH1A2
ALDH1A3
CD9
CD24
CD26
relative mRNA expression (-fold)
PS
DN
PCDME
PNaSS
D
(kDa)
75
50
50
SLC13A5
Actin
1
4.7
4.6
7.4
E
H&E
SLC13A5
F
intensity of SLC13A5 in immunostaining
positive area ratio (%)
G
(week)
#1
#2
#3
#4
PS dish
PNaSS gel
H
MSTO-211H
Total photon counts

Fig. 4

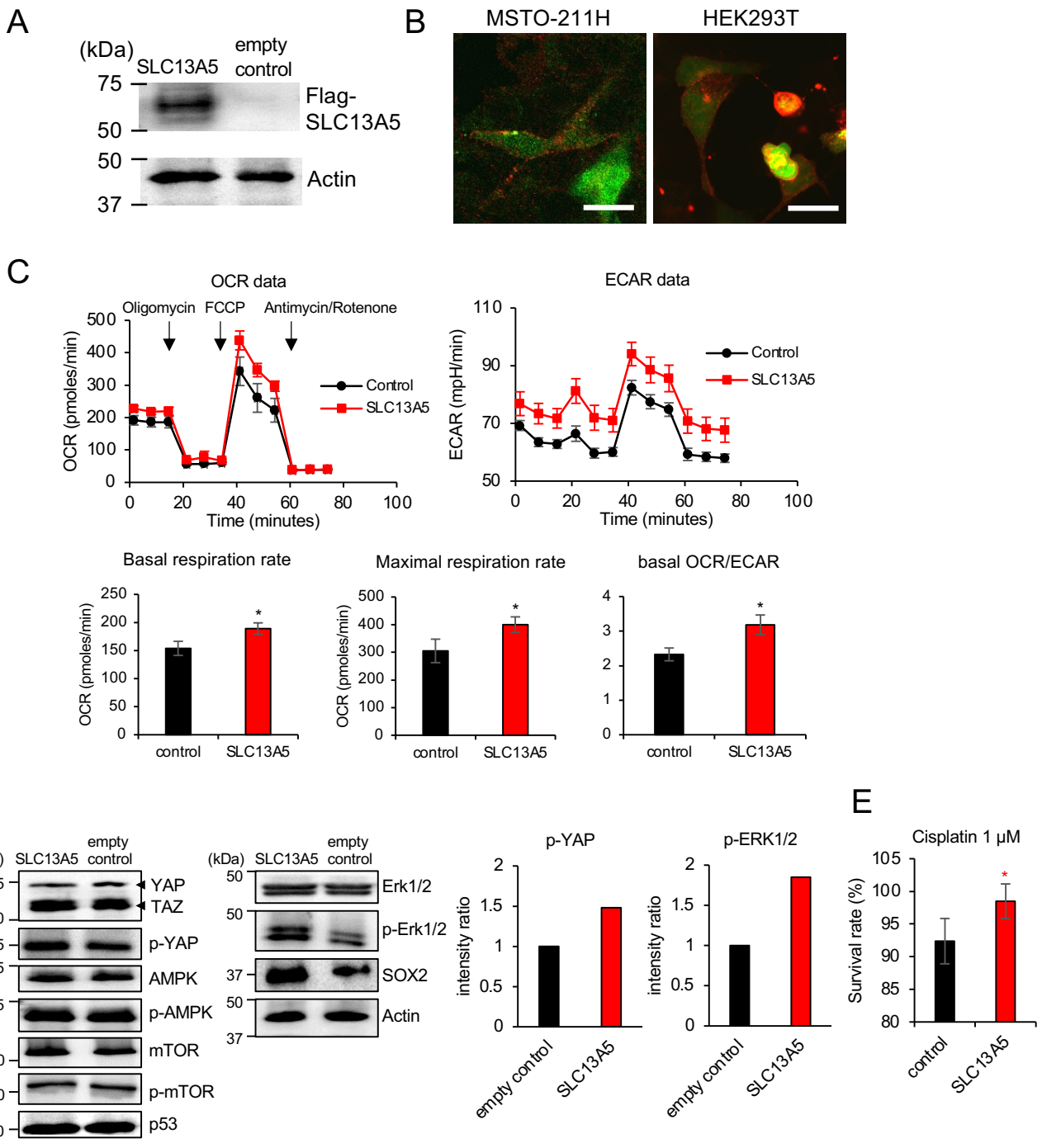
A
(kDa)
SLC13A5
empty control
75
50
50
37
Flag-SLC13A5
Actin
B
MSTO-211H
HEK293T
C
OCR data
Oligomycin
FCCP
Antimycin/Rotenone
OCR (pmoles/min)
Time (minutes)
Control
SLC13A5
ECAR data
ECAR (mpH/min)
Basal respiration rate
Maximal respiration rate
basal OCR/ECAR
control
SLC13A5
D
(kDa)
SLC13A5
empty control
YAP
TAZ
p-YAP
AMPK
p-AMPK
mTOR
p-mTOR
p53
Erk1/2
p-Erk1/2
SOX2
Actin
p-YAP
p-ERK1/2
intensity ratio
empty control
SLC13A5
E
Cisplatin 1 μM
Survival rate (%)
control
SLC13A5